Molecular Dynamics Simulations on the Mycotoxin Fumonisin B_1

Frank A. Momany[†] and Mary A. Dombrink-Kurtzman*[,‡]

Plant Polymer Research Unit and Mycotoxin Research Unit, National Center for Agricultural Utilization Research, Agricultural Research Service, U.S. Department of Agriculture, 1815 North University Street, Peoria, Illinois 61604-3902

The solution conformational properties of the mycotoxin fumonisin B_1 have been studied using molecular dynamics methodology. Fumonisins have been shown to inhibit sphinganine (sphingosine) *N*-acyltransferase (ceramide synthase) and show a wide range of toxic effects in many animals. This study of the solution properties of fumonisin B_1 attempts to add to the structural models necessary for the understanding of the binding and activity properties. The computational method uses a box with periodic boundaries, filled with explicit TIP3P water molecules, the substrate fumonisin B_1, and selected counterions for charge neutrality. The starting structure of fumonisin B_1 is added to the box by excluding water molecules. The explicit image method using 12-Å cutoffs is applied to the system and molecular dynamics are carried out on different starting conformations at 300 K in 100-picosecond (ps) steps. Examination of the resulting equilibrated conformations suggests that the structure is relatively extended and that previous computational studies in vacuo, showing a compact folded structure, may not be consistent with the solution structure.

Keywords: *Dynamics; fumonisin B_1; conformation; force field; mycotoxins*

INTRODUCTION

The mycotoxins "fumonisins" are produced by the corn fungal pathogens *Fusarium verticilliodes* (Sacc.) Niremberg (ex *F. moniliforme* Sheldon) and *F. proliferatum*, which are found in corn (maize) worldwide (*1*). Fumonisins represent a family of structurally related compounds. Fumonisin B_1 (FB_1), shown in Figure 1, is the most prevalent of the fumonisins in naturally contaminated corn and is usually present as 70% of the total fumonisins detected. Because FB_1 can occur in corn and corn-based products in the United States and has been associated with toxic effects in horses and pigs, the National Toxicology Program undertook a study in which rats and mice were exposed to FB_1 for two years. This long-term bioassay in F344/N rats and $B6C3F_1$ mice, which was recently completed, found FB_1 to be a renal carcinogen in male rats and a hepatocarcinogen in female mice (*2*). Post peer review of the final draft of the technical report is currently in progress.

In both in vivo and in vitro studies, fumonisins have been shown to inhibit sphinganine (sphingosine) *N*-acyltransferase (ceramide synthase), resulting in an increase in sphinganine in the de novo biosynthetic pathway of sphingolipids (*3* and reviewed in *4*). To date, four fumonisins, designated fumonisin B_{1-4} (FB_{1-4}), have been isolated and characterized as having biological activity, specifically because of their ability to inhibit ceramide synthase (*5*). FB_2, FB_3, and FB_4 vary structurally from FB_1 by the absence of a hydroxyl group(s) at C-10 and C-5 for FB_2 and FB_3, respectively, and at both C-5 and C-10 for FB_4. In addition, FA_{1-4} (acetyl amides of FB_{1-4}) have been described as lacking the ability to inhibit ceramide synthase (*5*). There are other structurally related fumonisin-type compounds, but because they are present as minor components, only limited study of them has been conducted.

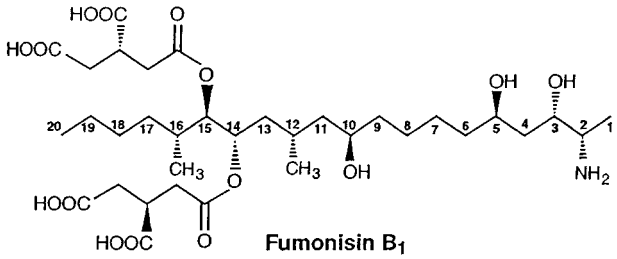

Figure 1. Absolute configuration of fumonisin B_1 (FB_1).

A variety of approaches using chemical derivatization methods have established the absolute stereochemistry of the backbone of FB_1 (reviewed in *6*). The relative configuration of FB_1 between C-1 and C-5 was determined by ApSimon et al. (*7*); that between C-5 and C-10, was determined by Hoye et al. (*8*); and that between C-10 and C-16, was determined by Blackwell et al. (*9*). The actual chirality present in the two side chain (at C-14 and C-15) tricarballylic acid esters was determined to have the *R* configuration (*10*), confirmed recently by Edwards et al. (*11*). All of the NMR data indicate that FB_1 adopts a linear configuration in aqueous solution, rather than a globular one (*6*).

Our goal in this work was to find an equilibrated solution structure of FB_1 that could be utilized in the determination of the binding of this molecule to site(s) associated with its enzyme inhibitory activity. Previous in vacuo calculations that attempted to determine the lowest energy structures of the FB_{1-4} mycotoxins had suggested that these molecules assume a cage-like or compact structure (*12*−*14*); however, these studies did not include dynamics simulations or the effects of solvent on the preferred conformations. Additionally, the

* To whom correspondence should be addressed. Telephone: (309) 681-6254. Fax: (309) 681-6686. E-mail: dombrink@mail.ncaur.usda.gov.

[†] Plant Polymer Research Unit.

[‡] Mycotoxin Research Unit.

10.1021/jf000842h
Published on Web 01/09/2001

absolute stereochemistry of the backbone of FB_1 (Figure 1) was used only for the last study (*14*) because it had not been determined at the time of the prior studies. For this reason, we have undertaken more rigorous computational studies of one (FB_1) of these interesting mycotoxins, using solution molecular dynamics simulations.

MATERIALS AND METHODS

All calculations were carried out using the modified AMBER (*15*) force field, and further modified as described (*16* and *17*) with the force field denoted AMB99C. The AMB99C force field was implemented in the Molecular Simulations Inc. (MSI) InsightII/4.0 Discover programs. In all calculations described here, the dielectric constant is treated as $\epsilon = 1$ with the electrostatic and nonbonded van der Waals 1−4 terms scaled by 0.5. Partial atomic charges of FB_1 were taken from electrostatic potential fitting of model ab initio data: all hydroxyl groups charges are H (0.430), O (−0.700), and C (0.270); carboxyl groups charges are O (−0.700), C′(0.679), and the carbon atom next to the C′ is C (−0.905); the amine group charges are NH3+ (0.905) and C (0.095); the ester group C═O charges are C′ (0.687), O (−0.492), −O− of (−0.300) and −O−C (0.200); finally, all hydrocarbon −CH2 and −CH3 groups charges are given 0.000 partial charge on each atom. All other hydrogen atoms are given 0.000 charge. Empirical energy minimization is carried out to a gradient of less than ∼0.001 kcal/mol using different minimization techniques, depending upon the size of the particular molecule or solvated system of interest. Molecular dynamics simulations were performed using the MSI Discover program. Integration is numerically carried out using the Verlet algorithm, and trajectories are initiated by assigning velocity components randomly selected from a thermal distribution at 300 K to the atoms. Calculations were carried out at 300 K, with the temperature controlled by a weak coupling to a temperature bath. Time steps of 1 fs were used to calculate velocities, but results were stored for examination at picosecond (ps) intervals. The equilibration time was approximately 1/10 of the total simulation time. Explicit hydrogen atoms are included in all calculations and both heavy atoms and hydrogen atoms are allowed to move on all molecules.

TIP3P water potentials are used throughout all simulations without internal constraints. A box with periodic boundaries is created to allow application of image conditions, and the molecule is placed in the box (example dimensions, 30 × 30 × 30 Å). Water molecules (∼850) and three Na^+ counterions are added to the box with the charged [four negatively charged carboxyl groups (tricarballylic acid) and one positively charged amine group] substrate, and energy minimization is carried out. The explicit image model with cutoff distances of 12 Å and a switching function with a buffer width of 2 Å were used for water boxes. This method does not require that the cutoffs be less than $^1/_2$ of the shortest unit cell length. After a short burst of molecular dynamics, and more energy minimization, a second attempt to add more water is made to fill any holes or void volume not previously filled. This procedure is continued until the density within the box is correct. The pressure in the box was monitored at the end of the equilibrium stage of dynamics, and the production steps were made running under constant pressure (PNT) conditions. Several simulations running for 100 ps are described in detail. The starting conformation of the FB_1 is changed in each step. The averaged results produced under constant pressure conditions were indistinguishable from constant volume results.

A starting conformation for FB_1 was obtained using a combination of dynamics simulations at elevated temperature (600 K) and structural preferences for allowed conformational space. Because of the manifold of minimum energy conformations corresponding to different values of the flexible torsional angles, we let the dynamic forces make the final decision as to the preferred position in solution. There may exist a residual conformational directing effect which is dependent upon the starting conformations, but this effect generally disappears shortly after a dynamics equilibration is achieved.

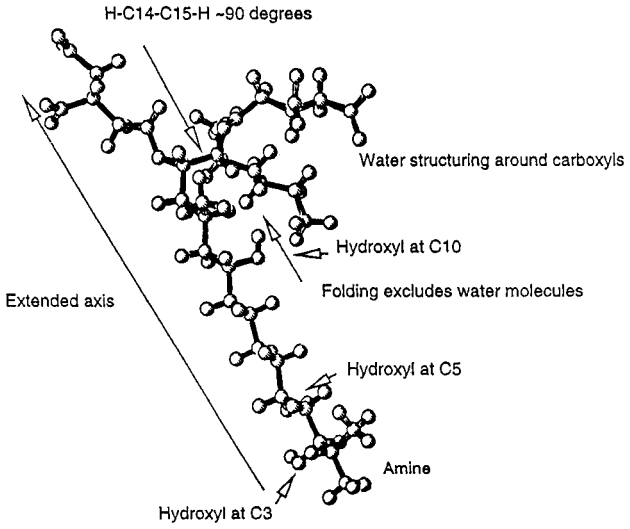

Figure 2. Conformation of FB_1 following a 200-ps simulation, with a starting conformation of nearly extended branches (at C-14 and C-15) and backbone (C-1 to C-20). The cell size for this Rep was 25 × 25 × 25 Å, just large enough to fit the extended molecule.

We describe herein results of solution dynamics simulations in which different dihedral angle positions are plotted over the time of the simulation. Different starting conformations were examined, and analyses of these dynamics steps are presented.

RESULTS AND DISCUSSION

Previous calculations in vacuo suggested that the FB_1 molecule is a compact folded structure (*12*−*14*). The previously observed conformations of low energy were found under vacuum conditions and so are biased by the uncharged state of the molecule and the lack of competing interactions with water (*12*−*14*). Blackwell et al. (*6*) have reported that all of their NMR data indicate that FB_1 adopts a linear conformation in aqueous solution, rather than a globular form; the linear conformation was observed, despite the possibility that hydrogen bonding may have occurred between the ester functions (at C-14 and C-15) and the hydrophilic end (C-1 to C-5). The vacuum state is most probably responsible for the compact, but perhaps unrealistic, structures. To overcome this situation and to provide insight into the mode of action of FB_1 at a molecular level, we relied on explicit water molecules to compete with the charged state of the FB_1 molecule and to shield the intermolecular charges from one another to give a realistic time-averaged conformation. We believe that a representation of the conformation available for biological receptors is found from these dynamic simulations at room temperature in solution.

In Figure 2 we plot a conformation of FB_1 taken from a 200-ps simulation with a starting conformation of nearly fully extended branches and backbone. The box size for this step was 25 × 25 × 25 Å, which is just large enough for the extended molecule to fit. During this simulation, a transient conformation of only a few picoseconds appeared in which the amine to tricarballylic acid distance was very short for both tricarballylic acid groups. This resulted from a bend in the main backbone chain bringing the amine group close to both acid groups simultaneously. One of the key dihedral

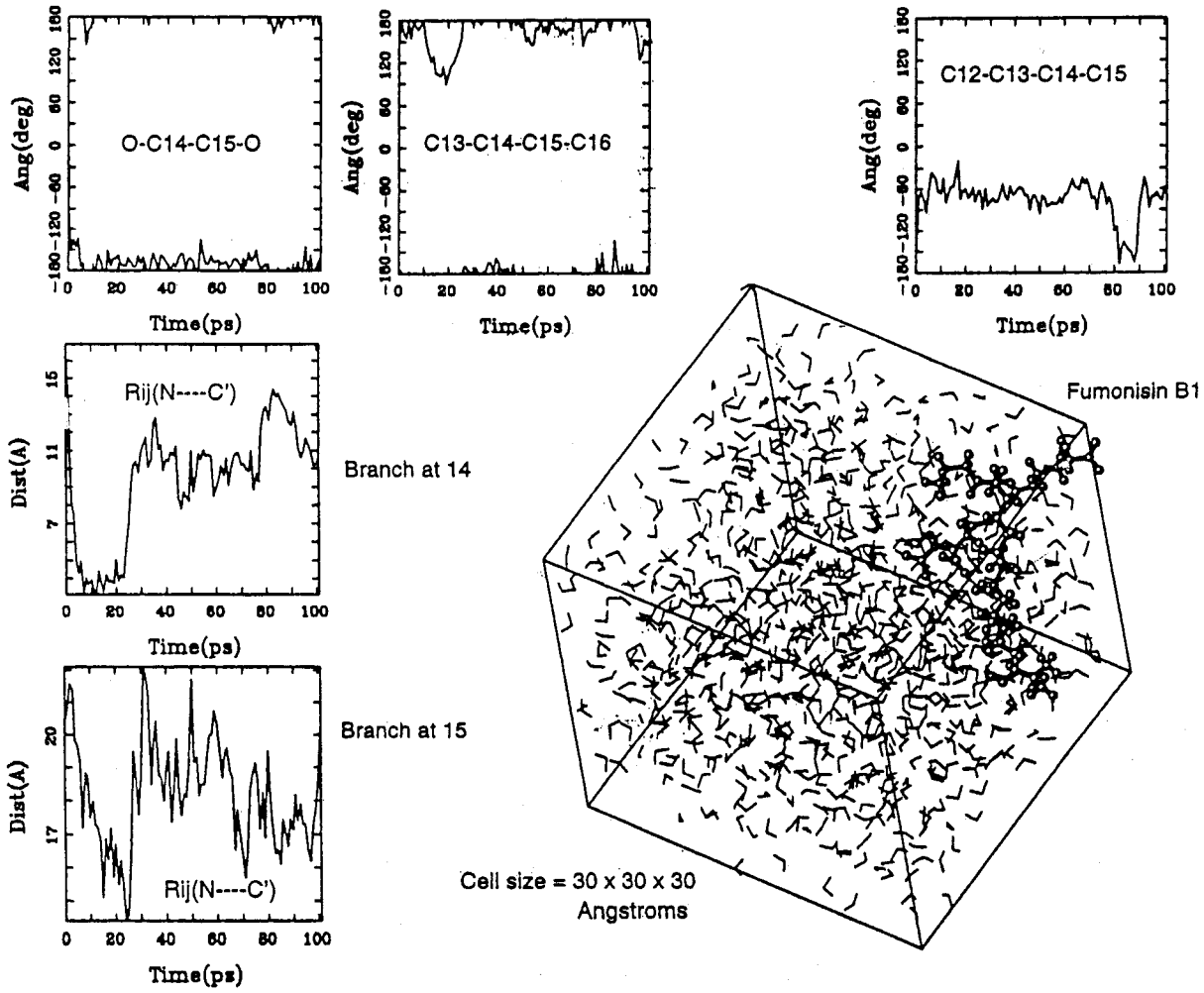

Figure 3. Plot of conformation of FB_1 following a 100-ps simulation in a cell size of 30 × 30 × 30 Å. Dihedral angles are given for O−C14−C15−O; C13−C14−C15−C16; C12−C13−C14−C15. Distances are shown for (N- - - -C′) branches at C14 and C15.

angles, O−C14−C15−O, also underwent a considerable conformational transition over the time course of the simulation, starting at an extended state, ∼180°, moving to gauche minus (∼−60°) at about 40 ps and changing to the gauche plus (∼+50°) conformation at ∼150 ps. There is only slight preference for the gauche minus state over the gauche plus conformational state as seen from the time of occupation of each conformation. It was of interest to examine the image cells for this step to see how the parent molecule was interacting with the images. This is important in the case of FB_1 because it is a long zwitterionic-like molecule with a basic group at one end of the chain and four charged carboxyl groups at the other branched ends. If the molecule stretches across the cell (in this step the cell was 25 × 25 × 25 Å), it is possible for the head and tails to strongly interact with the molecular images in the surrounding cells and energetically drive the preferred conformation to an extended form, as we see occurred in the step described here. In fact, an infinite chain is formed by close contacts between the oppositely charged polar headgroups from image cells on each side of the 0th cell, and these interactions played a decisive role in the FB_1 conformations observed for this cell size, even though there are three competing Na^+ counterions in solution. Because of this technical problem, we expanded the cell such that end-to-end interactions between both ends of the FB_1 molecule and its images cannot take place.

The second simulation, described next, better reproduces a dilute solution even though molecular dimer formation is still possible. The cell size was expanded to 30 × 30 × 30 Å, and at that size, close hydrogen bonding contacts between images on opposite sides of the cell are impossible. One must be aware that during the dynamics the counterions may leave the vicinity of the parent FB_1 molecule and find similar close contacts with the image molecules. This movement of ions is acceptable but may be somewhat confusing to the reader. The path of folding in the larger cell, occurring over a 100-ps dynamics simulation, is shown in Figure 3. It is clear that the folding is a combination of several factors. First, the charged groups play a role in organizing the solvent around the FB_1 molecule in the region of C-10 to C-20 (Figure 4a). There are generally six water molecules interacting with each carboxyl group, while one water molecule forms a bridge between the two close carboxyl groups (Figure 4a). Another water molecule bridges between a carboxyl group and the ester C═O oxygen atom, and another bridging of water molecules occurs between a C-15 branch carboxyl group and the C-10 hydroxyl group (Figure 4a). The total solvent organization around the acid group acts as a polar negative wall pointing away from the groups; the water molecules align with their polar positive (partial charge) hydrogen atoms toward the negative charges on the acid group (Figure 4a). The net negative charge, at each end of the C-14 and C-15 branches, results in

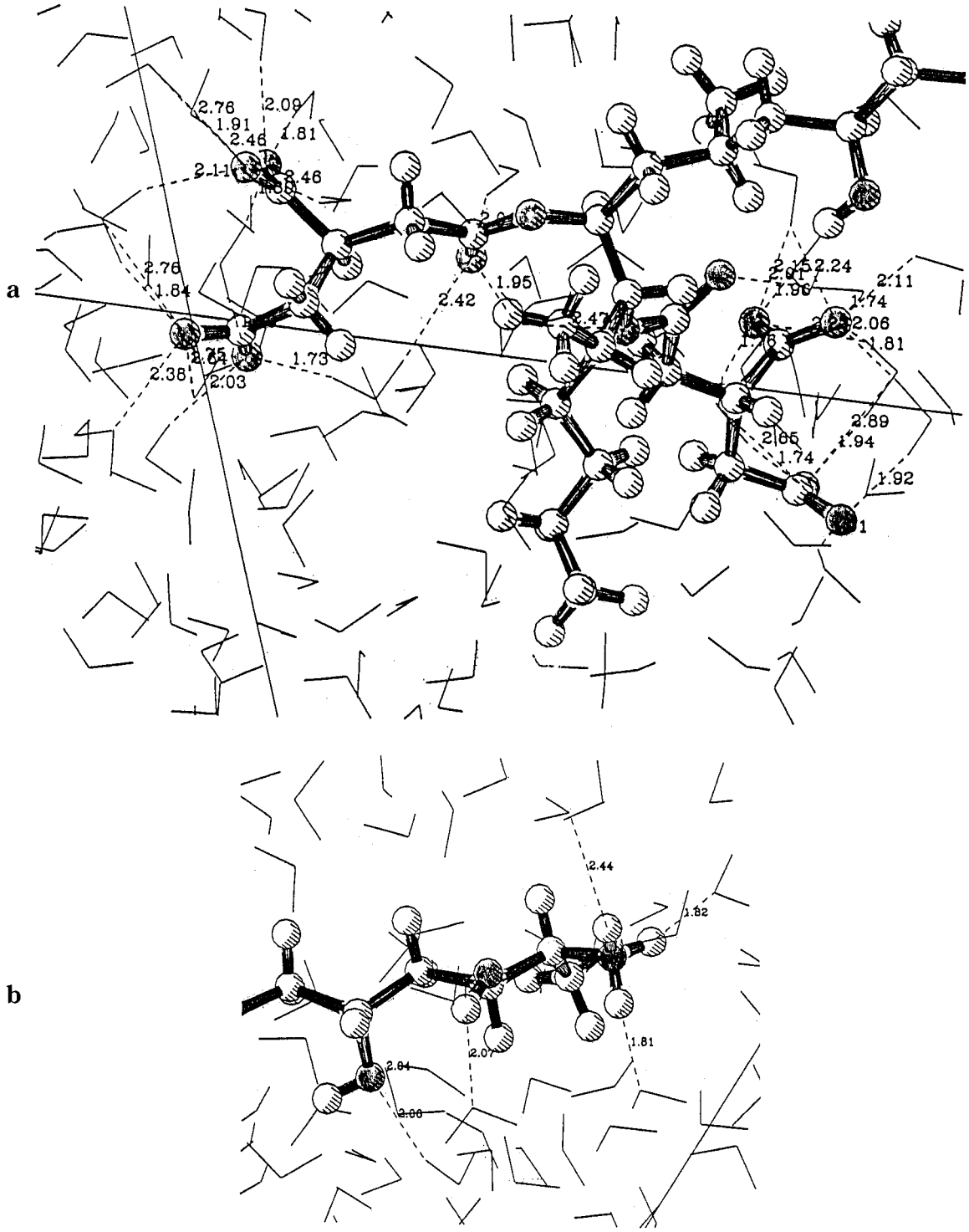

Figure 4. Water molecules interacting around FB_1 for the region of C-10 to C-20 (a). Charged groups play a role in organizing solvent molecule; generally six water molecules interact with each carboxyl group. The total solvent organization around the acid groups acts as a polar negative wall pointing away from the group. The net negative charge, at each end of the C-14 and C-15 branches, results in the tricarballylic groups being repelled from one another. For the region of C-1 to C-6 (b), the C-2 amine and the C-3 and C-5 hydroxyl groups form hydrogen bonds with water. The oxygen atoms are lightly shaded, and the nitrogen atom is darkened.

the tricarballylic groups being repelled from one another. For the region of C-1 to C-6, the C-2 amine and the C-3 and C-5 hydroxyl groups form hydrogen bonds with water (Figure 4b).

A second solvation effect is the attempt to remove as much of the hydrocarbon section of the chain from contact with the solvent as possible. This hydrophobic effect is well-known, and the length of the hydrocarbon chain in FB_1 is sufficient for the force field to attempt to bury some of the nonpolar groups inside a polar cap. The result is a partially folded conformation (Figure 3), with the path by which the final structure was achieved depicted in the time vs molecular parameter frames. Several dihedral angles (Figure 3) have changed as the simulation proceeded; they are shown as a function of the time course of the simulation. The distances between the tricarballylic groups and the amine group are also shown as a function of the time course of the simulation

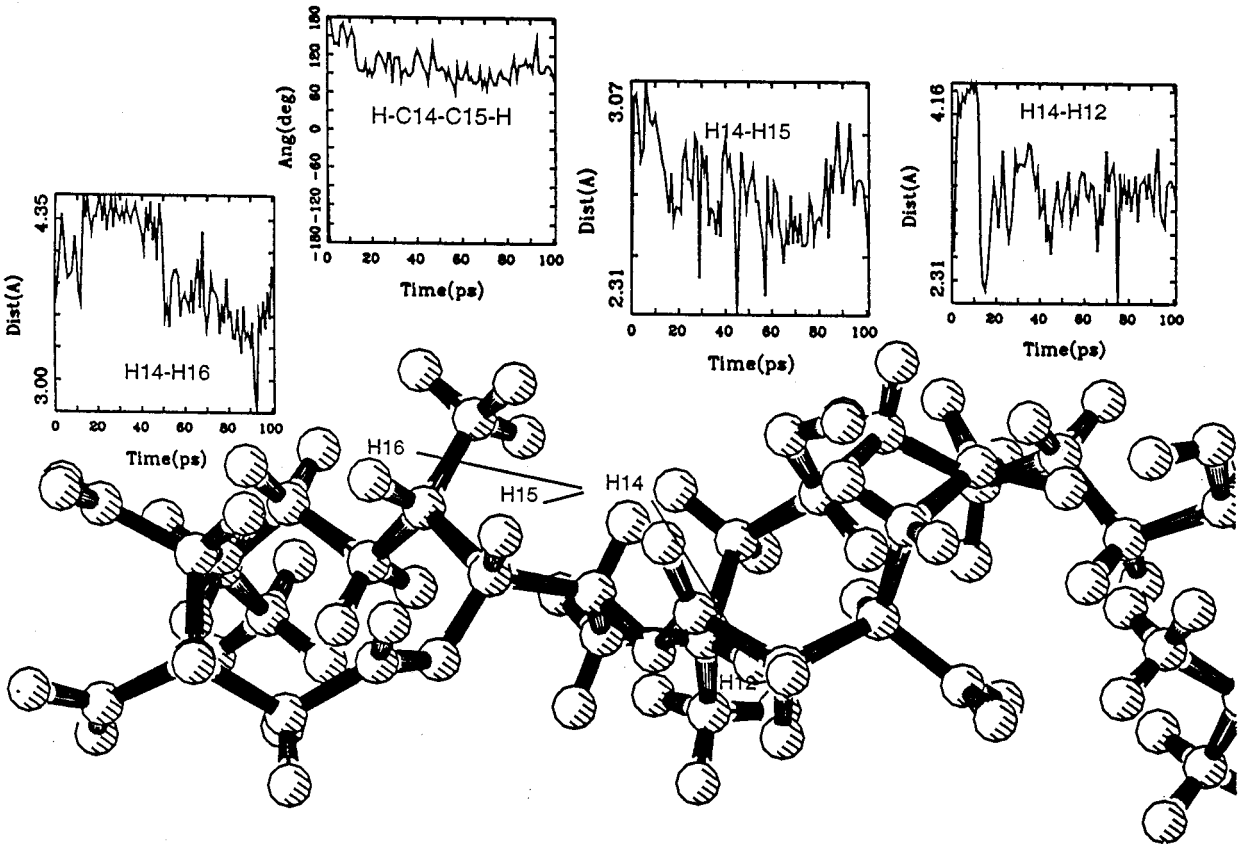

Figure 5. Time frames of various distances (H14−H16, H14−H15, and H12−H14) and dihedral angle (H−C14−C15−H) for comparison of the results of dynamics simulations of FB_1 to experimental $J_{H,H}$ coupling constants and available nOes.

(Figure 3). The very short starting distance between the C-14 branch acid and the C-2 amine quickly changed to a distance of 11−12 Å.

From the starting FB_1 structure, the molecule has, over 100 ps of dynamics, undergone a conformational transition in which the main chain, atoms C-1 to C-14, is nearly fully extended, and the chain from C-16 to C-20 has folded toward the C-15 branched ester linkage. The result is that the longest extended stretch is between the amine on C-2 and the carboxyl group on the C-14 branched ester linkage (Figure 2).

NMR Coupling Constants and Nuclear Overhauser Enhancement Comparisons. It is productive to compare the results of the dynamics simulations of FB_1 to experimental $J_{H,H}$ coupling constants and available nOes. We show the time frames of various distances (Figure 5) and dihedral angles (Figures 5 and 6) for which both coupling data and nuclear Overhauser enhancements have been published. Blackwell et al. (*6* and *9*) reported $J_{H,H}$ coupling constants for FB_1 and derivatives of FB_1. For FB_1, they reported coupling constants of 2.4 and 10.8 Hz for H-13,H-14, 3.7 Hz for H-14,H-15, and 8.1 Hz for H-15,H-16. In the case of H-13,H-14, the two values (2.4, 10.8 Hz) suggest that there are both trans and gauche interactions, which is consistent with our finding of a trans backbone heavy atom conformation at this bond. The value for the H-14,H-15 coupling is small (3.7 Hz), suggesting a value of $\varphi \sim 100°$, which is consistent with the time vs dihedral angle for this bond (Figure 5) where the dihedral angle varies between ∼80° and 120° over the last 80 ps of the simulation. Using the alkyl Karplus relationship (*18*) for calculating the coupling constant, one obtains a value near 3 Hz for this region of dihedral space, and when corrected for the electronegativity effect, it is somewhat larger, ∼3.5 Hz, in good agreement with the experimental value of 3.7 Hz. The coupling constant for the H-15,H-16 interaction (8.1 Hz) would imply a dihedral angle value of ∼150°. The time profile of the simulation for the H−C15−C16−H dihedral angle is shown in Figure 6. Clearly, after about 50 ps, the conformation has flipped from a starting value of ∼−60° to an equilibrium between +60° and 180°. It is obvious from Figure 6 that the near trans conformation at the C15−C16 bond is becoming more occupied as the simulation proceeds.

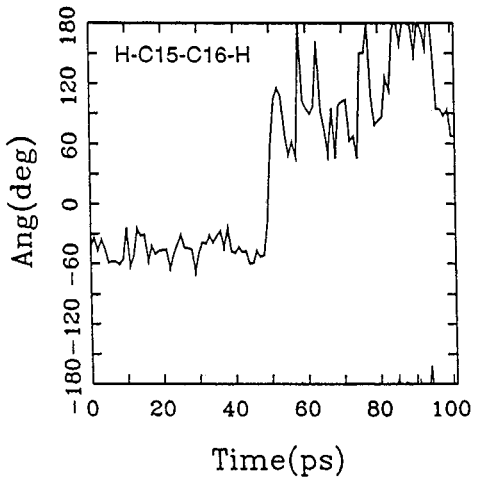

Figure 6. Time frames of dihedral angle (H−C15−C16−H) for comparison of the results of dynamics simulations of FB_1 to experimental $J_{H,H}$ coupling constants and available nOes.

Blackwell et al. (*6* and *9*) also report several nOes associated with close contact of hydrogen atoms. Of

particular interest is the H14−H16 distance shown in Figure 5. We again see the conformational transition at ∼50 ps to a close contact of ∼3.5 Å. This is the same time period that was described above for the H−C15−C16−H dihedral angle. This would suggest that the observed nOe for H14−H16 (*6* and *9*) is allowed for this conformation. Another nOe of interest is that found for H14−H15, across the bond, and of average distance of ∼2.7 Å in this simulation. Finally, the H12−H14 distance profile for the observed nOe between these atoms is shown in Figure 5, with an average simulation distance of ∼3.2 Å. We do not have estimates from the NMR results for the distances or magnitudes of the nOes, only that nOes were observed for those H- - -H contacts described above. For the reasons cited above, we believe that the conformation occurring during the time period after 50 ps had elapsed is a conformation close to that observed experimentally in CD_3OD (*6* and *9*). The molecular dynamics simulations of FB_1 are in good agreement with the experimental observations.

Comparison to Previous Calculations. Stereo models of the FB_{1-4} molecules from previous calculations performed in vacuo (*12*−*14*) suggested that there exists a compact folded conformation in which the backbone section from C-1 to C-15 folds toward both the C-14 and the C-15 branch propane-1,2,3-tricarboxylic acid side chains. This folding creates a cage-like structure with all the charged groups located near the C-2 amine end. Clearly, localized carboxyl charged groups have considerable repulsive electrostatic energy and will not come in close contact with one another if they are not restrained or charge shielded. Although it may be assumed that in vacuo hydroxyl groups of FB_1 may form intraresidue and interresidue hydrogen bonds, in the presence of solvent molecules, hydrogen bonds form between solute (FB_1) and solvent (H_2O). In our simulations of solution conformational properties of FB_1, the water molecules act as a solvent shield, which is similar to increasing the dielectric constant. We do not find any stable compact structures during the molecular dynamics simulations in solution.

LITERATURE CITED

(1) Nelson, P. E.; Desjardins, A. E.; Plattner, R. D. Fumonisins, mycotoxins produced by *Fusarium* species: biology, chemistry and significance. *Ann. Rev. Phytopathol.* **1993**, *31*, 233−252.

(2) National Toxicology Program. Toxicology and carcinogenesis studies of fumonisin B_1 (CAS No. 116355-83-0) in F344/N rats and $B6C3F_1$ mice (feed studies); National Institutes of Environmental Health Sciences, Summary Report TR-496. U.S. Government Printing Office: Washington, DC, 1999; pp 1−4.

(3) Wang, E.; Norred, W. P.; Bacon, C. W.; Riley, R. T.; Merrill, A. H., Jr. Inhibition of sphingolipid biosynthesis by fumonisins. Implications for diseases with *Fusarium moniliforme*. *J. Biol. Chem.* **1991**, *266*, 14486−14490.

(4) Merrill, A. H., Jr; Liotta, D. C.; Riley, R. T. Fumonisins: fungal toxins that shed light on sphingolipid function. *Trends Cell Biol.* **1996**, *6*, 218−223.

(5) Norred, W. P.; Plattner, R. D.; Dombrink-Kurtzman, M. A.; Meredith, F. I.; Riley, R. T. Mycotoxin-induced elevation of free sphingoid bases in precision-cut rat liver slices: specificity of the response and structure−activity relationships. *Toxicol. Appl. Pharmacol.* **1997**, *147*, 63−70.

(6) Blackwell, B. A.; Edwards, O. E.; Fruchier, A.; ApSimon, J. W.; Miller, J. D. NMR structural studies of fumonisin B_1 and related compounds from *Fusarium moniliforme*. In *Fumonisins in Food*; Jackson, L. S., DeVries, J. W., Bullerman, L. B., Eds.; Plenum Press: New York, 1996; pp 75−91.

(7) ApSimon, J. W.; Blackwell B. A.; Edwards, O. E.; Fruchier, A. Relative configuration of the C-1 to C-5 fragment of fumonisin B_1. *Tetrahedron Lett.* **1994**, *35*, 7703−7706.

(8) Hoye, T. R.; Jimenez, J. I.; Shier, W. T. Relative and absolute configuration of the fumonisin B_1 backbone. *J. Am. Chem. Soc.* **1994**, *116*, 9409−9410.

(9) Blackwell, B. A.; Edwards, O. E.; ApSimon, J. W.; Fruchier, A. Relative configuration of the C-10 to C-16 fragment of fumonisin B_1. *Tetrahedron Lett.* **1995**, *36*, 1973−1976.

(10) Boyle, C. D.; Kishi, Y. Absolute configuration at the tricarballylic acid moieties of fumonisin B_1 and AAL toxin T_A. *Tetrahedron Lett.* **1995**, *36*, 5695−5698.

(11) Edwards, O. E.; Blackwell, B. A.; Driega, A. B.; Bensimon, C.; ApSimon, J. W. The absolute stereochemistry of the ester functions of fumonisin B_1. *Tetrahedron Lett.* **1999**, *40*, 4515−4518.

(12) Beier, R. C.; Elissalde, M. H.; Stanker, L. H. Calculated three-dimensional structures of the fumonisin B_{1-4} mycotoxins. *Bull. Environ. Contam. Toxicol.* **1995**, *54*, 479−487.

(13) Beier, R. C.; Elissalde, M. H.; Stanker, L. H. Molecular modeling studies of the fumonisin mycotoxins. In *Immunoassays for Residue Analysis*: *Food Safety*; Beier, R. C., Stanker, L. H., Eds.; ACS Symposium Series 621, American Chemical Society: Washington, DC, 1996; pp 368−385.

(14) Beier, R. C.; Stanker, L. H. Molecular models for the stereochemical structures of fumonisin B_1 and B_2. *Arch. Environ. Contam. Toxicol.* **1997**, *33*, 1−8.

(15) Cornell, W. D.; Cieplak, P.; Bayly, C. I.; Gould, I. R.; Merz, K. M., Jr.; Ferguson, D. M.; Spellmeyer, D. C.; Fox, T.; Caldwell, J. W.; Kollman, P. A. A second generation force field for the simulation of proteins, nucleic acids, and organic molecules. *J. Am. Chem. Soc.* **1995**, *117*, 5179−5197.

(16) Momany, F. A.; Willet, J. L. Computational studies on carbohydrates: in vacuo studies using a revised AMBER force field, AMB99C, designed for α-(1→4) linkages. *Carbohydr. Res.* **2000**, *326*, 194−209.

(17) Momany, F. A.; Willet, J. L. Computational studies on carbohydrates: solvation studies on maltose and cyclomaltooligosaccharides (cyclodextrins) using a DFT/ab initio-derived empirical force field, AMB99C. *Carbohydr. Res.* **2000**, *326*, 210−226.

(18) Haasnoot, C. A. G.; de Leeuw, F. A. A. M.; Altona, C. The relationship between proton−proton − NMR coupling constants and substituent electronegativities − I. An empirical generalization of the Karplus equation. *Tetrahedron* **1980**, *36*, 2783−2792.

Received for review July 7, 2000. Revised manuscript received November 6, 2000. Accepted November 7, 2000.

JF000842H